Repulsively induced photon superbunching in driven resonator arrays

T. Grujic,[1,*] S. R. Clark,[1,2] D. Jaksch,[1,2] and D. G. Angelakis[2,3,†]
[1]*Clarendon Laboratory, University of Oxford, Parks Road, Oxford OX1 3PU, UK*
[2]*Centre for Quantum Technologies, National University of Singapore, 2 Science Drive 3, Singapore 117542*
[3]*Science Department, Technical University of Crete, Chania, Crete, Greece, 73100*
(Received 13 December 2012; published 29 May 2013)

We analyze the nonequilibrium behavior of driven nonlinear photonic resonator arrays under the selective excitation of specific photonic many-body modes. Targeting the unit-filled ground state, we find a counterintuitive "superbunching" in the emitted photon statistics in spite of relatively strong on-site repulsive interaction. We consider resonator arrays with Kerr nonlinearities described by the Bose-Hubbard model, but also show that an analogous effect is observable in near-future experiments coupling resonators to two-level systems as described by the Jaynes-Cummings-Hubbard Hamiltonian. For the experimentally accessible case of a pair of coupled resonators forming a photonic molecule, we provide an analytical explanation for the nature of the effect.

DOI: 10.1103/PhysRevA.87.053846 PACS number(s): 42.50.Pq, 05.30.Rt, 64.70.Tg

I. INTRODUCTION

Coupled resonator arrays (CRAs) offer the intriguing possibility of realizing strongly correlated many-body quantum states of light. Early work on CRAs assumed idealized, lossless arrays and focused in particular on equilibrium quantum phase transitions in these structures. However, near-future photonic devices will necessarily operate under driven-dissipative conditions on account of unavoidable photon loss, thereby serving as natural platforms for the exploration of novel nonequilibrium many-body photonic effects [1–9]. Our understanding of these systems is in its infancy, making it desirable to concretely connect the nonequilibrium properties of CRAs with their more familiar equilibrium structure. To this end, there have been recent efforts to identify signatures of the equilibrium quantum phase transition as originally proposed in Refs. [10–18] which survive under lossy dynamics.

We propose an alternative scheme to chart different regions of parameter space and connect nonequilibrium observables to the underlying Hamiltonian properties. We envisage a resonator array driven to a nonequilibrium steady state (NESS) by external lasers, with the laser frequency chosen such that the unit-filled equilibrium ground state is selectively addressed and populated. By "unit-filled ground state" we mean the lowest-lying eigenstate of the undriven CRA in the subspace spanned by states with as many photons as there are resonators. Features arising from the details of the nonequilibrium operation appear in collected emission statistics, including a counterintuitive many-body repulsion-induced bunching of the emitted photons, the magnitude of which is controllable via tuning Hamiltonian parameters. Novel superbunched light sources far exceeding the bunching of thermal photons may find important applications in ghost imaging technologies [19] and all-optical simulation of two-photon correlations in quantum walks [20].

In this work we first focus on a minimal-sized two-site resonator system. Such dimers or photonic molecules are expected to be experimentally viable in the near future in different technologies ranging from semiconductors to circuit QED. We initially study the system for resonator nonlinearities of the repulsive Kerr-type, as shown in Fig. 1(a), to illustrate our driving scheme. We then analyze the Jaynes-Cummings type encountered when resonator modes interact with embedded effective two-level systems [21], as in Fig. 1(b). We note here that we have previously investigated the validity of modeling the Jaynes-Cummings-Hubbard (JCH) with the simpler, single species Bose-Hubbard (BH) model [22] and accordingly also demonstrate that the superbunching signature persists under a JCH description. Moving beyond this minimal "array," bunched emission is also demonstrated in near-future experimentally accessible mesoscopic-sized systems [23,24].

II. SYSTEM

We consider a one-dimensional chain of M coupled single-mode optical resonators under periodic boundary conditions. Each resonator of frequency ω_c is coherently coupled to its two nearest neighbors. External lasers coherently drive each resonator in phase with amplitude Ω. In a frame rotating at the laser frequency ω_L, the system Hamiltonian is

$$\hat{\mathcal{H}}^{(M)} = \sum_{j=1}^{M}[\Delta_c \hat{a}_j^\dagger \hat{a}_j + U\hat{a}_j^\dagger \hat{a}_j^\dagger \hat{a}_j \hat{a}_j + \Omega(\hat{a}_j^\dagger + \hat{a}_j)] - J\sum_{\langle j,j'\rangle}(\hat{a}_j^\dagger \hat{a}_j'). \quad (1)$$

Here U is the Kerr nonlinear strength, J is the photon hopping rate, Ω is the photon driving strength, and $\langle j,j'\rangle$ denotes nearest-neighbor resonators. We take all Hamiltonian coupling rates to be much smaller than the bare resonator frequency: $U,J,\Omega \ll \omega_c$. The operators $\hat{a}_j$ are the photon destruction operators for the photon mode in resonator j. The detuning of the driving laser frequency from the bare cavity frequency is $\Delta_c = \omega_c - \omega_L$.

Markovian photon loss processes from each cavity are incorporated via a quantum master equation formalism for the evolution of the system density matrix ρ, $\dot{\rho} = \mathcal{L}^{(M)}[\rho]$,

*t.grujic1@physics.ox.ac.uk
†dimitris.angelakis@gmail.org

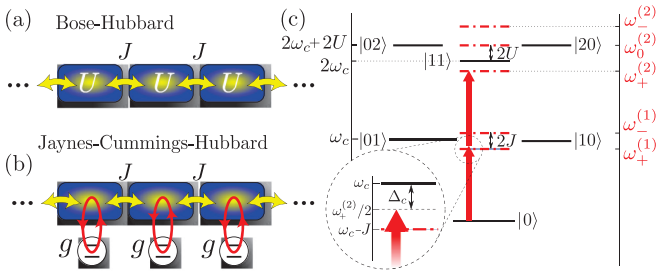

FIG. 1. (Color online) (a) Schematic of driven-dissipative Bose Hubbard model, featuring local coherent driving, photon tunneling, and a purely photonic Kerr nonlinearity. (b) The driven-dissipative Jaynes-Cummings model with effective photon nonlinearity generated by couplings to two-level systems. (c) Diagram showing bare basis (solid black) and eigenfrequencies (dash dotted red) of the driven system for the minimal system of $M = 2$ resonators. The laser is tuned so that two laser photons (vertical red arrows) are capable of promoting the system to the lowest-lying two-photon state.

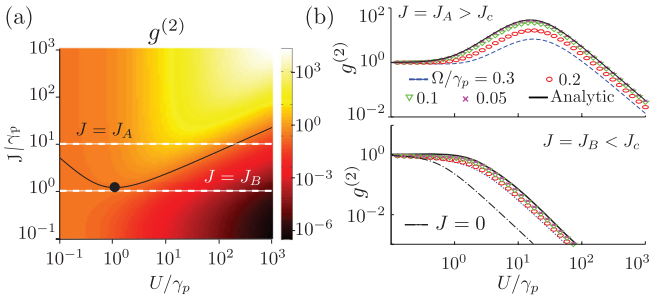

FIG. 2. (Color online) (a) Emitted photon statistics as a function of J and U for a dimer ($M = 2$) of resonators driven according to Eq. (3). Driving strength $\Omega/\gamma_p = 0.3$. Black curve: analytic result for $g^{(2)} = 1$. Black dot: the point $(J_c/\gamma_p, U_c/\gamma_p)$ where bunching sets in. (b) "Slices" along the dotted lines in panel (a) above and below the critical hopping amplitude at which the bunching feature appears, for decreasing driving strengths, down to the infinitesimal limit (solid black lines).

where

$$\mathcal{L}^{(M)}[\rho] = \frac{1}{i}[\hat{\mathcal{H}}^{(M)}, \rho] + \gamma_p \sum_{j=1}^{M} \hat{\mathcal{D}}_{\hat{a}_j}[\rho]. \tag{2}$$

The dissipative part of the dynamics is described by $\hat{\mathcal{D}}_{\hat{a}_j}[\rho] = \hat{a}_j \rho \hat{a}_j^\dagger - \frac{1}{2}(\hat{a}_j^\dagger \hat{a}_j \rho + \rho \hat{a}_j^\dagger \hat{a}_j)$. The NESS of the system is described by the density matrix $\rho_{\rm ss}$ which satisfies $\mathcal{L}[\rho_{\rm ss}] = 0$. Intraresonator observables are measured with respect to this state, $\langle \hat{O} \rangle_{\rm ss} \equiv {\rm Tr}(\hat{O}\rho_{\rm ss})$, and may be experimentally inferred from measurements on the emitted photons using existing techniques.

III. TWO-RESONATOR "DIMER"

We begin by analyzing the simplest possible driven resonator array consisting of just $M = 2$ resonators, which serves to illustrate clearly our scheme for accessing the unit-filled ground state. Figure 1(b) shows the low-lying eigenstructure of the undriven Hamiltonian of Eq. (1) for $M = 2$, and our driving scheme. The two one-photon eigenfrequencies are the symmetric (+) and antisymmetric (−) Bloch modes and lie (in the bare frame, with $\Omega = 0$) at $\omega_\pm^{(1)} = \omega_c \mp J$, with corresponding eigenstates $|1_\pm\rangle$. The two-photon eigenfrequencies are $\omega_0^{(2)} = 2\omega_c + 2U$, $\omega_\pm^{(2)} = 2\omega_c + U \mp \sqrt{U^2 + 4J^2}$, with eigenstates $|2_0\rangle$, $|2_\pm\rangle$, respectively. The unit-filled ground state is of frequency $\omega_+^{(2)}$. This mode undergoes a qualitative change between the extreme limits of a localized state, characterized by vanishing on-site photon number fluctuation ${\rm Var}(\hat{a}_j^\dagger \hat{a}_j) \to 0$ for $U \gg J$, to a coherent superposition state with ${\rm Var}(\hat{a}_j^\dagger \hat{a}_j) \to \frac{1}{2}$ for $U \ll J$. For increasing system size, the behavioural transition of the ground state becomes sharper, approaching the celebrated Bose-Hubbard Mott-insulating-to-superfluid phase transition in the infinite-system limit [25].

To selectively populate the unit-filled ground state of Eq. (1) for a particular set of Hamiltonian parameters, we set the driving laser frequency such that two laser photons are resonant with the lowest-lying two-photon mode, i.e., $2\omega_L = \omega_+^{(2)}$, implying a laser detuning

$$\Delta_c(J,U) = \tfrac{1}{2}(\sqrt{U^2 + 4J^2} - U). \tag{3}$$

We note that Δ_c can assume values in the range $[0, J]$, and so a laser with bandwidth J centered on the resonator frequency will allow an exploration of all nonlinearities U. Fixing $\Delta_c = \Delta_c(J,U)$ for a given hopping and nonlinearity, we now examine which features of the underlying Hamiltonian mode structure leave fingerprints on experimentally accesible photonic observables. In our nonequilibrium setting the photon number is not an integer and the photon number variance is not an informative order parameter. To compensate for these nonequilibrium effects, we instead focus on the local zero-time photon correlation function $g^{(2)} \equiv g_j^{(2)} = \langle \hat{a}_j^\dagger \hat{a}_j^\dagger \hat{a}_j \hat{a}_j \rangle_{\rm ss} / \langle \hat{a}_j^\dagger \hat{a}_j \rangle_{\rm ss}^2$, a statistical quantity directly accessible in CRA setups through standard methods like homodyne detection. We note that $g^{(2)}$ measurements may be particularly valuable in weakly driven systems, where the excitation number may be very small, but normalized statistical quantities may be collected over longer times.

Figure 2(a) shows $g^{(2)}$ measured in the NESS of a BH dimer pumped at the laser detuning of Eq. (3) for a range of tunneling rates and nonlinearities (J,U). Results are obtained via exact diagonalization of the matrix representation of the superoperator $\mathcal{L}^{(M)}$, with the steady-state density matrix $\rho_{\rm ss}$ reconstructed from the zero-eigenvalue eigenvector after enforcing the unit-trace condition. The diagram is broadly divided into three regions, defined by Poissonian ($g^{(2)} \approx 1$), antibunched ($g^{(2)} < 1$), and bunched ($g^{(2)} > 1$) statistics. Notably, there is a critical coupling rate $J_{\rm crit}$ between the resonators below which bunching does not occur for any value of nonlinearity, suggesting that the bunching arises from a cooperative many-body effect in the NESS. Figure 2(b) shows the qualitative difference in the behavior of the correlation function above and below this critical point. For comparison, an isolated resonator driven at its single-particle (unit-filled) resonance never exhibits bunched signatures [see dash-dotted line in lower panel of Fig. 2(b)].

At low nonlinearities $U \ll \gamma_p$, the dimer is driven at the frequency of the zero-momentum Bloch mode, and its response

is approximately linear. The NESS is a coherent state, inheriting Poissonian statistics with $g^{(2)} = 1$, and average population $\langle \hat{a}_j^\dagger \hat{a}_j \rangle = (2\Omega/\gamma_p)^2$, for all J. At the other extreme, taking the hardcore limit $U \gg \gamma_p$ (while also remaining in the regime $U \ll \omega_c$), no more than a single photon per resonator can be injected, and the problem is reduced to two coupled two-level systems whose emission is completely antibunched ($g^{(2)} = 0$), with mean excitation number per resonator $\lim_{U\to\infty}\langle \hat{a}^\dagger \hat{a} \rangle = x(2x+1)/[(2x+1)^2 + xy]$, where $x \equiv (2\Omega/\gamma_p)^2$ and $y \equiv (J/\Omega)^2$.

Away from these extreme limits, in the region of parameter space where J and U are comparable, the emitted light is bunched for hopping rates larger than a critical rate $J > J_c$. This is counterintuitive, as we are probing a two-photon state with significant repulsion favoring separation, and yet we find an enhanced probability of photons being emitted together, relative to the statistics of the driving. This physics is reminiscent of many-boson bound states and localized breather modes in the Bose-Hubbard model [26–30]; however, we show below that our bunching is qualitatively different.

We derive features of this bunched region by considering the limit of infinitesimal driving. Figure 2(b) shows that the correlation function approaches a limiting behavior as $\Omega/\gamma_p \to 0$, an observation confirmed by perturbatively expanding the elements of the NESS density matrix ρ_{ss} in increasing powers of the driving strength, then solving for $g^{(2)}$ [8]. Details are presented in the appendix. The equations thus obtained are physically opaque; however, further progress can be made by making a pure-state ansatz $\rho_{ss} = |\Psi_{ss}\rangle\langle\Psi_{ss}|$, valid in the low-driving regime [7]. The state $|\Psi_{ss}\rangle$ is found as the stationary state (corresponding to the zero eigenvalue) of the effective Hamiltonian $\hat{\mathcal{H}}_{\text{eff}}^{(M)}$ obtained by replacing $\Delta_c \to \Delta_c - i\gamma_p/2$ in Eq. (1), which may be interpreted as the Hamiltonian governing a single quantum trajectory, with a vanishing probability of a quantum jump ensured by taking the limit $\Omega/\gamma_p \to 0$.

Considering only the lowest excitations and exploiting the symmetry of the two-site system, we set $|\Psi_{ss}\rangle = C_{00}|00\rangle + C_1(|01\rangle + |10\rangle) + C_{11}|11\rangle + C_2(|02\rangle + |20\rangle)$, from which the correlation function follows as $g^{(2)} = |C_2|^2/|C_1|^4$. We obtain the minimum resonator coupling for which bunched statistics appear as $\tilde{J}_c = J_c/\gamma_p = [(3+2\sqrt{2})/4]^{1/2}$, and the nonlinearity at this point $\tilde{U}_c = U_c/\gamma_p = \sqrt{\tilde{J}_c}$ as marked in Fig. 2(a). The full calculation and expressions for the coefficients C are presented in the appendix. The transition from super- to sub-Poissonian statistics (i.e., where $g^{(2)} = 1$) is found to occur at $\tilde{J} \approx (\tilde{U}/2)^{1/2}$ for $J \gg J_c$, while for very large but finite U/J, the exact solution may be simplified to $g^{(2)} \approx (\frac{\tilde{J}}{\tilde{U}})^2(1 + 4\tilde{J}^2)$.

Figure 3 offers physical insight into this phenomenon, showing the emission spectrum of the system as calculated from the Fourier transform $S(\omega - \omega_L)$ of the on-site steady-state autocorrelation function $S(\tau) = \langle \hat{a}^\dagger(t+\tau)\hat{a}(t)\rangle$, as a function of increasing nonlinearity. The resonator coupling is sufficiently large ($J/\gamma_p = 10 > \tilde{J}_c$) to observe bunched emission [top panel of Fig. 3(a)]. At all nonlinearities, the spectrum is dominated by two bright features. These correspond to decays from the lower and upper one-particle states $|1_\mp\rangle$ to the vacuum $|0\rangle$, labeled lines A and B, respectively.

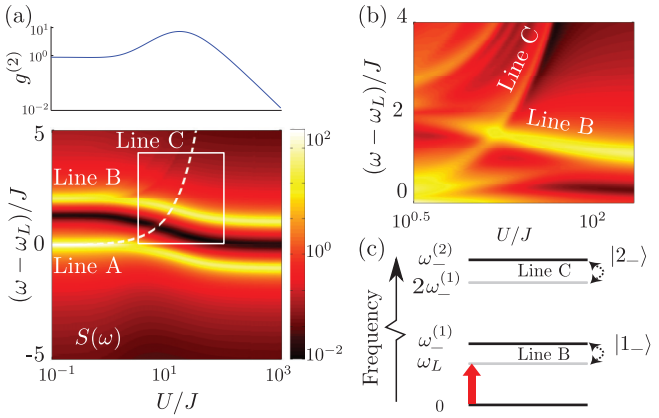

FIG. 3. (Color online) (a) Lower: Emission spectral function relative to the laser frequency $|S(\omega - \omega_L)|^2$ with increasing nonlinearity U at a fixed hopping $J/\gamma_p = 10$. At our weak driving ($\Omega/\gamma_p = 0.3$), the spectrum is dominated by transitions between the vacuum and one-particle manifold (bright lines A and B). Weaker features involving the two-particle manifold are also present; for instance, the dashed curve highlighting line C. Upper: the zero-time correlation function $g^{(2)}$. (b) Closer view of the region of parameter space bounded by the white box in panel (a) but calculated at the higher driving $\Omega/\gamma_p = 1$ to highlight the crossing of the features labeled Lines B and C. (c) Transitions involved in spectral lines B and C, with only the relevant modes drawn.

Weaker features are also present, which do not significantly affect the steady-state photon populations, but may strongly modify statistical quantities such as $g^{(2)}$. Line C in Figs. 3(a) and 3(b) corresponds to emission from the highest two-particle state $|2_+\rangle$ to an intermediate level, as drawn in Fig. 3(c). In the vicinity of the crossing of emission lines B and C at $\tilde{U}/\tilde{J} = (9 - \sqrt{17})/4$, the population in $|2_-\rangle$ reaches a maximum, as photons emitted as part of the line B decay process may transfer population instead to $|2_-\rangle$. We now calculate the properties of the modes $|2_\pm\rangle$ by diagonalizing the Hamiltonian of Eq. (1) at zero driving $\Omega = 0$. In the Fock basis, we find the normalized forms

$$|2_-\rangle = \frac{-\sqrt{2}\Delta_c|11\rangle + J(|02\rangle + |20\rangle)}{\sqrt{2\Delta_c(2\Delta_c + U)}},$$

$$|2_+\rangle = \frac{\sqrt{2}(\Delta_c + U)|11\rangle + J(|02\rangle + |20\rangle)}{\sqrt{2(\Delta_c + U)(2\Delta_c + U)}}.$$

Defining $\Pi_\alpha, \alpha \in \{-,0,+\}$ as the ratio of the projections of the mode $|2_\alpha\rangle$ into the space spanned by the states $\{|20\rangle, |02\rangle\}$ to the projection into the distributed state $|11\rangle$, we find $\Pi_- < \frac{1}{2}$ always, while $\Pi_+ > \frac{1}{2}$. The analogous ratio for coherent light is $\Pi_{\text{coh}} = \frac{1}{2}$.

There is therefore a greater probability of finding the two photons of the mode $|2_-\rangle$ in the same resonator than distributed between them, relative to the driven $|2_+\rangle$ mode. This is reflected in the enhanced probability of simultaneous emission of two photons ($g^{(2)} > 1$) around this crossing. In contrast the mode $|2_+\rangle$ favors delocalising its two photons relative to the statistics of the driving laser. Thus, we observe either approximately coherent, or antibunched light in all regions of parameter space except in the vicinity of the crossing of lines B and C. This underlying mechanism makes the photon

bunching qualitatively different from that of discrete breather modes in dissipative nonlinear lattices [31,32].

For resonator couplings $J < \gamma_p$, the global physics of the system resembles that of an isolated nonlinear resonator driven at its resonance frequency, such that antibunching is always expected—in spectral terms, the crossing of lines B and C is hidden inside the coalesced lines A and B.

IV. LARGER SYSTEMS

We now investigate how the correlations presented in Fig. 2(b) evolve as the system size increases, continuing to drive the commensurately filled ground state. An analytic approach valid for arbitrary Hamiltonian couplings beyond $M = 2$ resonators is intractable. Instead, we numerically calculate the eigenvector of the effective Hamiltonian $\hat{\mathcal{H}}_{\rm eff}^{(M)}$ with eigenvalue closest to zero (taking a series of successively weaker drivings Ω/γ_p to ensure convergence of observables). Exploiting the translational invariance of systems with periodic boundary conditions allows us to access systems of up to $M = 7$ resonators while retaining three photons per resonator in simulations.

Figure 4 shows the evolution of the counterintuitive bunched region for increasing system sizes up to $M = 7$ resonators. We see a reduction in the magnitude and range of interaction strengths for which bunched light is observed as the system size increases. The bunching region is seen to retreat up the J axis, while smaller interaction strengths U are necessary to induce the bunching. This explains the reduction in the magnitude of the effect observed for cross sections at constant resonator coupling, as in Fig. 4(a).

Rigorous quantum trajectory calculations based on the matrix product state representation and the time-evolving block decimation algorithm [33–35] performed at a finite driving strength broadly agree with the results obtained via numerically exact diagonalization of $\hat{\mathcal{H}}_{\rm eff}^{(M)}$, as presented in Fig. 5.

We solve for NESS observables in the trajectory formalism by first finding the unit-filled ground-state frequencies $\omega_-^{(M)}$ via imaginary time evolution of a unit-filled matrix product state (MPS). The steady state of a system is then obtained

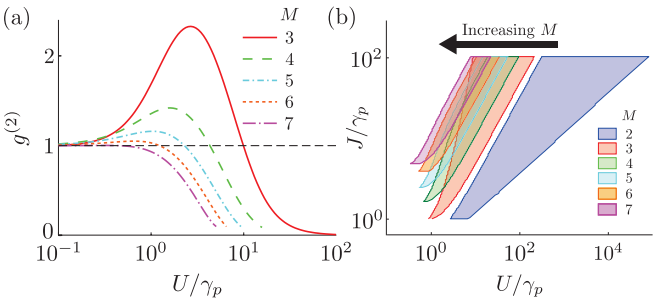

FIG. 4. (Color online) (a) Correlation function evaluated as a function of increasing nonlinearity at fixed resonator coupling $J/\gamma_p = 10^1$. Note the $M = 2$ results are not included as the bunching in this case is significantly larger. (b) Extent of the bunched region in (J,U) parameter space, as measured from $U = U_{\rm LHS}$ corresponding to the peak $g^{(2)}$, to $U = U_{\rm RHS}$ at which the correlations change from bunched to antibunched, for a range of resonator couplings J.

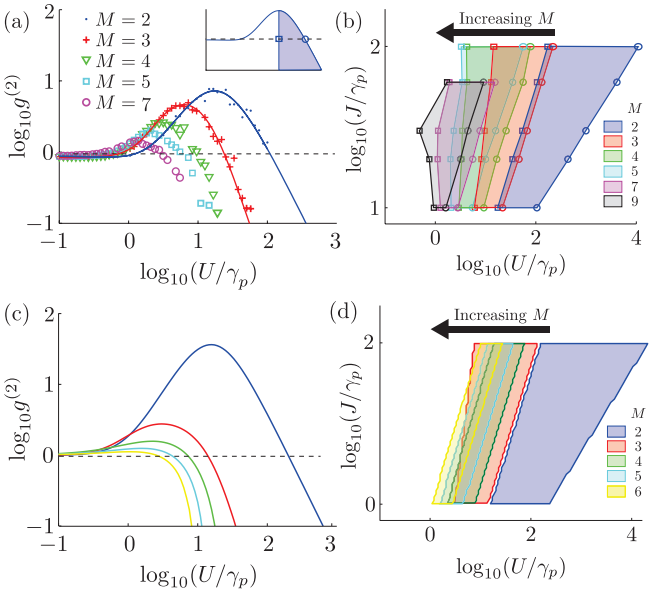

FIG. 5. (Color online) (a) Evolution of a slice along line $J = J_A$ through diagram of Fig. 2(a) for increasing system size, at fixed hopping $J/\gamma_p = 10$ and driving $\Omega/\gamma_p = 0.4$. The solid blue and red lines are exact-diagonalization results for small systems. Inset illustrates the metric we use for the width of the bunching region in panel (b)—squares denote the maximum bunching, and circles show where the correlation function crosses from bunched to antibunched at $g^{(2)} = 1$. (b) Evolution of extent of bunching region in parameter space for increasing system size. Note that, in these calculations, we assumed open boundary conditions, in contrast to the periodic boundaries used in the main article. For comparison, panels (c) and (d) show results obtained by finding the stationary states of the effective quantum trajectory Hamiltonian $\hat{\mathcal{H}}^{(M)}$.

by driving at the frequency $\omega_-^{(M)}/M$ by evolving a matrix-product-operator representation of the system density matrix in real time using the time-evolving block decimation (TEBD) algorithm under the action of Eq. (2) in the main text. Consistency between the two stages of the computation is ensured by using the same MPS truncation parameter χ in both the ground-state and trajectory calculations.

Figure 5 shows full trajectory results for system sizes up to $M = 9$. Each point corresponds to an average over 20 trajectories, and each trajectory is itself averaged over 15 000 time steps. All calculations used a matrix product state parameter $\chi = 60$. This figure shows that the bunched emission discussed in the main text also occurs for larger system sizes M at finite driving amplitude. The phenomenon is therefore robust and may be expected in finite-sized experimental arrays. We also see that the precise features of the bunching region do depend on drive strength, as already observed for $M = 2$ in Fig. 2(b).

V. PHOTON STATISTICS IN JAYNES-CUMMINGS ARRAYS

Near-future circuit QED systems will most probably realize a few-photon resonator nonlinearity via a Jaynes-Cummings interaction with embedded two-level systems [10], as described by the Jaynes-Cummings-Hubbard Hamiltonian in a

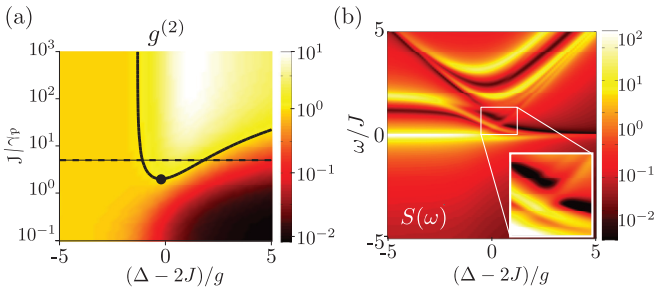

FIG. 6. (Color online) Steady-state observables for a two-site Jaynes-Cummings array, driven at its lowest two-particle resonance. Parameters: $g/\gamma_p = 10$. (a) Zero-time photon correlation as a function of resonator coupling J and atom-resonator detuning Δ, playing the part of an effective photon nonlinearity. (b) Spectral function $|S(\omega)|^2$ evaluated along the dashed line in panel (a), again showing a crossing of emission lines promoting photons to a state with enhanced probability of bunched emission.

rotating frame:

$$\hat{\mathcal{H}}^{(M)}_{\rm JCH} = \sum_{j=1}^{M}[\Delta_c \hat{a}_j^\dagger \hat{a}_j + (\Delta_c - \Delta)\hat{\sigma}_j^+\hat{\sigma}_j^- + \Omega(\hat{a}_j^\dagger + \hat{a}_j)] + g\sum_{j=1}^{M}(\hat{a}_j^\dagger\hat{\sigma}_j^- + \hat{a}_j\hat{\sigma}_j^+) - J\sum_{\langle j,j'\rangle}(\hat{a}_j^\dagger\hat{a}_j'). \quad (4)$$

Here $\Delta = \omega_c - \omega_a$ denotes the difference between the resonators' frequency and the TLS transition frequency, g is the Jaynes-Cummings coupling strength, and $\hat{\sigma}^\pm$ denote two-level-system (TLS) raising and lowering operators. The JCH is known to possess a localized-delocalized transition as either the hopping J is increased, or the Jaynes-Cummings parameter Δ is made more negative. This transition is similar in some respects to the phase transition of the BH model, although it also differs in fundamental ways on account of the different nature of the systems' intrinsic excitations (bosons and polaritons, respectively) [14–18,22].

Figure 6 presents evidence that the mechanism underlying the bunched emission discussed above in the context of a the driven Bose-Hubbard model persists in this qualitatively different setting for realistic atom-resonator couplings and loss rates and is therefore observable in near-future state-of-the art experiments involving just two coupled resonators.

VI. CONCLUSIONS

We have proposed the selective excitation of photonic many-body modes of interest in open resonator arrays using external driving lasers, over which we have full control of frequency and amplitude. We have shown how a combination of the equilibrium Hamiltonian structure and nonequilibrium operation lead to an interaction-induced region of bunched emission. This feature was found to persist in mesoscopic-sized arrays and is also found under a more realistic array description, making its observation feasible in coming experiments.

APPENDIX A: DENSITY-MATRIX SOLUTION FOR TWO-SITE BOSE-HUBBARD SYSTEM

Here we explicitly solve for the steady-state density-matrix elements of the driven-dissipative two-site system described by Eq. (1) under driving and dissipation. That is, we solve for $\rho_{\rm ss}$ satisfying $\mathcal{L}^{(M)}[\rho_{\rm ss}] = 0$ in a minimal basis consisting of states with at most two photons in the system, where the superoperator $\mathcal{L}^{(M)}$ is defined in Eq. (2) of the main text. We recursively solve for density-matrix elements at increasing powers of the weak driving strength Ω/γ_p, as in Ref. [8].

For notational convenience, we label the basis states in the following way: $|0\rangle \to 1$, $|10\rangle \to 2$, $|01\rangle \to 3$, $|11\rangle \to 4$, $|20\rangle \to 5$, $|02\rangle \to 6$. The symmetry of our system under exchange of resonators $1 \Leftrightarrow 2$ allows for a considerable reduction in the necessary size of the density-matrix description. The assumption that the system is very weakly driven is embodied in the assumption $\rho_{11} \approx 1$.

Following the approach in Ref. [8], we derive equations involving increasing orders of the driving strength Ω/γ_p, with the goal of calculating $g^{(2)} = \rho_{55}^2/\rho_{22}$. Here we give solutions for the elements ρ_{55} and ρ_{22}, which in turn depend on other elements:

$$\rho_{55} = \frac{\Omega}{2\gamma_p[(2\gamma_p)^2 + (2U)^2 + (4J)^2]} \times \big[\mathrm{Im}(\rho_{25})8\sqrt{2}\big(\gamma_p^2 + U^2 + 2J^2 - JU\big) + \mathrm{Re}(\rho_{25})8\sqrt{2}\gamma_p J - \mathrm{Im}(\rho_{24})8J(-2J+U) - \mathrm{Re}(\rho_{24})8\gamma_p J\big].$$

The elements ρ_{24} and ρ_{25} are given by

$$\rho_{24} = \Omega\frac{2\sqrt{2}J(\sqrt{2}\rho_{22} - \rho_{15}) - i(2\rho_{22} - \rho_{14})\left(i\Delta_c + iJ + 2iU - \frac{3}{2}\gamma_p\right)}{\left(i\Delta_c + iJ - \frac{3}{2}\gamma_p\right)\left(i\Delta_c + iJ + 2iU - \frac{3}{2}\gamma_p\right)},$$

$$\rho_{25} = \Omega\frac{\sqrt{2}J(2\rho_{22} - \rho_{14}) + i(\rho_{15} - \sqrt{2}\rho_{22})\left(i\Delta_c + iJ - \frac{3}{2}\gamma_p\right)}{\left(i\Delta_c + iJ - \frac{3}{2}\gamma_p\right)\left(i\Delta_c + iJ + 2iU - \frac{3}{2}\gamma_p\right)}.$$

These depend on the elements ρ_{14} and ρ_{15} which are proportional to the vacuum-state population, to first order in the driving

$$\rho_{14} = \frac{4J\Omega + 2i\Omega(\gamma_p - 2i\Delta_c - 2iU)}{(\gamma_p - 2i\Delta_c)(\gamma_p - 2i\Delta_c - 2iU) + 4J^2}\frac{\left(1 + \frac{2i(\Delta_c - J)}{\gamma_p}\right)}{1 + \left(\frac{2(\Delta_c - J)}{\gamma_p}\right)^2}\left(\frac{2i\Omega}{\gamma_p}\right)\rho_{11},$$

$$\rho_{15} = \frac{2\sqrt{2}J\Omega + \sqrt{2}i\Omega(\gamma_p - 2i\Delta_c)}{(\gamma_p - 2i\Delta_c)(\gamma_p - 2i\Delta_c - 2iU) + 4J^2}\frac{\left(1 + \frac{2i(\Delta_c - J)}{\gamma_p}\right)}{1 + \left(\frac{2(\Delta_c - J)}{\gamma_p}\right)^2}\left(\frac{2i\Omega}{\gamma_p}\right)\rho_{11}.$$

Meanwhile the denominator of $g^{(2)}$ is given by

$$\rho_{22} = \left(\frac{2\Omega}{\gamma_p}\right)^2 \frac{1}{1+\left(\frac{2(\Delta_c - J)}{\gamma_p}\right)^2}\rho_{11}.$$

The correlation function $g^{(2)}$ does not appear to be amenable to physical insight or meaningful mathematical manipulation. Instead, in the following section we employ a pure-state wave-function ansatz for the state of the system, i.e., setting $\rho_{\rm ss} \equiv |\Psi_{\rm ss}\rangle\langle\Psi_{\rm ss}|$ and observing that, at weak driving, the purity of the steady-state density matrix is $\mathrm{Tr}(\rho_{\rm ss}^2) \approx 1$.

APPENDIX B: WAVE-FUNCTION ANSATZ SOLUTION

We now make the ansatz $|\Psi_{\rm ss}\rangle = C_{00}|00\rangle + C_1(|01\rangle + |10\rangle) + C_{11}|11\rangle + C_2(|02\rangle + |20\rangle)$ and find the zero eigenvector of the effective-trajectory Hamiltonian obtained by replacing the resonator frequency by $\omega_c \to \omega_c - i\gamma/2$ in the Bose-Hubbard dimer Hamiltonian. We find the following results for the wave-function coefficients, after exploiting the symmetry of the system by setting $C_{02} = C_{20} \equiv C_2$ and $C_{01} = C_{10} \equiv C_1$:

$$C_{00} \approx 1,$$
$$C_1 = -\frac{\Omega C_{00}}{\Delta_c - J - i\frac{\gamma}{2}},$$
$$C_2 = -\frac{\Omega C_1}{\sqrt{2}(\Delta_c + U - i\gamma_p/2)}\left(\frac{J}{\Delta_c - i\gamma_p/2} + 1\right),$$
$$\times\left[1 - \frac{J^2}{(\Delta_c - i\gamma_p/2)(\Delta_c + U - i\gamma_p/2)}\right]^{-1}.$$

From these we may explicitly obtain the correlation function as $g^{(2)} = 2|C_2|^2/|C_1|^4 = 2|C_2/C_1^2|^2$ as

$$g^{(2)} = \frac{1}{\left|1 + \frac{AU}{A^2 - J^2}\right|^2},$$

where $A = \Delta_c - i\gamma_p/2$. To solve for the parameters $(\tilde{U}, \tilde{J})_{\rm crit} \equiv (U_{\rm crit}/\gamma_p, J_{\rm crit}/\gamma_p)$ at which bunching sets in, we set $g^{(2)} = 1$ and additionally implicitly differentiate the resulting expression, setting $d\tilde{J}/d\tilde{V} = 0$, to find the result

$$\tilde{J}_{\rm crit} = \tilde{U}_{\rm crit}^4 = \sqrt{\frac{3 + 2\sqrt{2}}{4}}.$$

We may also obtain the limiting dividing line $\tilde{J}_d = \tilde{J}_d(\tilde{U})$ tracing the crossing from super- to sub-Poissonian statistics ($g^{(2)} = 1$) for large hopping rates $J \gg \gamma_p$ as

$$\lim_{\tilde{J}\gg 1} \tilde{J}_d = \sqrt{\frac{\tilde{U}}{2}}.$$

[1] I. Carusotto, D. Gerace, H. E. Tureci, S. De Liberato, C. Ciuti, and A. Imamoğlu, Phys. Rev. Lett. **103**, 033601 (2009).
[2] D. Angelakis, S. Bose, and S. Mancini, Europhys. Lett. **85**, 20007 (2009).
[3] A. Tomadin, V. Giovannetti, R. Fazio, D. Gerace, I. Carusotto, H. E. Türeci, and A. Imamoglu, Phys. Rev. A **81**, 061801 (2010).
[4] S. Schmidt, D. Gerace, A. A. Houck, G. Blatter, and H. E. Türeci, Phys. Rev. B **82**, 100507 (2010).
[5] T. C. H. Liew and V. Savona, Phys. Rev. Lett. **104**, 183601 (2010).
[6] M. J. Hartmann, Phys. Rev. Lett. **104**, 113601 (2010).
[7] M. Bamba, A. Imamoğlu, I. Carusotto, and C. Ciuti, Phys. Rev. A **83**, 021802 (2011).
[8] S. Ferretti, L. C. Andreani, H. E. Türeci, and D. Gerace, Phys. Rev. A **82**, 013841 (2010).
[9] M. Knap, E. Arrigoni, W. von der Linden, and J. H. Cole, Phys. Rev. A **83**, 23821 (2011).
[10] D. G. Angelakis, M. F. Santos, and S. Bose, Phys. Rev. A **76**, 31805 (2007).
[11] A. Greentree, C. Tahan, J. Cole, and L. Hollenberg, Nat. Phys. **2**, 856 (2006).
[12] D. Rossini and R. Fazio, Phys. Rev. Lett. **99**, 186401 (2007).
[13] J. Hartmann, Nat. Phys. **2**, 849 (2006).
[14] M. Aichhorn, M. Hohenadler, C. Tahan, and P. B. Littlewood, Phys. Rev. Lett. **100**, 216401 (2008).
[15] S. Schmidt and G. Blatter, Phys. Rev. Lett. **103**, 86403 (2009).
[16] J. Koch and K. Le Hur, Phys. Rev. A **80**, 023811 (2009).
[17] S. Schmidt and G. Blatter, Phys. Rev. Lett. **104**, 216402 (2010).
[18] A. Mering, M. Fleischhauer, P. A. Ivanov, and K. Singer, Phys. Rev. A **80**, 053821 (2009).
[19] M. I. Kolobov, *Quantum Imaging* (Springer, Berlin, 2007).
[20] A. Peruzzo, M. Lobino, J. Matthews, N. Matsuda, A. Politi, K. Poulios, X. Zhou, Y. Lahini, N. Ismail, K. Wörhoff *et al.*, Science **329**, 1500 (2010).
[21] J. Fink, M. Göppl, M. Baur, R. Bianchetti, P. Leek, A. Blais, and A. Wallraff, Nature (London) **454**, 315 (2008).
[22] T. Grujic, S. R. Clark, D. Jaksch, and D. G. Angelakis, New J. Phys. **14**, 103025 (2012).
[23] A. Houck, H. Türeci, and J. Koch, Nat. Phys. **8**, 292 (2012).
[24] A. Majumdar, A. Rundquist, M. Bajcsy, V. D. Dasika, S. R. Bank, and J. Vučković, Phys. Rev. B **86**, 195312 (2012).
[25] D. Jaksch, C. Bruder, J. I. Cirac, C. W. Gardiner, and P. Zoller, Phys. Rev. Lett. **81**, 3108 (1998).
[26] A. Scott, J. Eilbeck, and H. Gilhøj, Phys. D **78**, 194 (1994).
[27] V. Fleurov, R. Schilling, and S. Flach, Phys. Rev. E **58**, 339 (1998).
[28] S. Aubry, S. Flach, K. Kladko, and E. Olbrich, Phys. Rev. Lett. **76**, 1607 (1996).
[29] G. Kalosakas and A. R. Bishop, Phys. Rev. A **65**, 043616 (2002).
[30] K. Winkler, G. Thalhammer, F. Lang, R. Grimm, J. Denschlag, A. Daley, A. Kantian, H. Büchler, and P. Zoller, Nature (London) **441**, 853 (2006).
[31] P. Maniadis and S. Flach, Europhys. Lett. **74**, 452 (2007).
[32] D. Zueco, P. J. Martínez, L. M. Floría, and F. Falo, Phys. Rev. E **71**, 036613 (2005).
[33] G. Vidal, Phys. Rev. Lett. **91**, 147902 (2003).
[34] G. Vidal, Phys. Rev. Lett. **93**, 040502 (2004).
[35] S. R. White and A. E. Feiguin, Phys. Rev. Lett. **93**, 076401 (2004).